JGR Space Physics

RESEARCH ARTICLE
10.1029/2019JA026596

MAVEN-IUVS Observations of the CO_2^+ UV Doublet and CO Cameron Bands in the Martian Thermosphere: Aeronomy, Seasonal, and Latitudinal Distribution

J.-C. Gérard[1], L. Gkouvelis[1], B. Ritter[1], B. Hubert[1], S. K. Jain[2], and N. M. Schneider[2]

[1]LPAP, STAR Institute, Université de Liège, Liège, Belgium, [2]LASP, University of Colorado Boulder, Boulder, CO, USA

Key Points:
- The peak altitudes of the CO_2+ UVD and CO Cameron dayglow are strongly correlated and indicators of the changing overlying CO_2 column
- The altitude and the shape of the dayglow limb profiles are well modeled outside dust storm periods using the MCD neutral atmosphere
- The upward shift of the peak altitudes of both emissions by up to 20 km during the dust storm season is underestimated by the model

Correspondence to:
J.-C. Gérard,
jc.gerard@uliege.be

Citation:
Gérard, J.-C., Gkouvelis, L., Ritter, B., Hubert, B., Jain, S. K., & Schneider, N. M. (2019). MAVEN-IUVS observations of the CO_2^+ UV doublet and CO Cameron bands in the Martian thermosphere: Aeronomy, seasonal, and latitudinal distribution. *Journal of Geophysical Research: Space Physics*, *124*, 5816–5827. https://doi.org/10.1029/2019JA026596

Received 8 FEB 2019
Accepted 3 JUN 2019
Accepted article online 11 JUN 2019
Published online 4 JUL 2019

Abstract We analyze two Martian years of dayglow measurements of the CO Cameron bands and the CO_2^+ ultraviolet doublet (UVD) at 298–299 nm with the Imaging UltraViolet Spectrograph on board the Mars Atmosphere and Volatile EvolutioN (MAVEN) orbiter. We show that the altitude and the brightness of the two emissions peaks are strongly correlated, although data were collected over a wide range of latitudes and seasons. Averaged limb profiles are presented and compared with numerical simulations based on updated calculations of the production of the CO ($a^3\Pi$) and the CO_2^+ ($B\ ^2\Sigma$) states. The model simulations use the solar flux directly measured on board MAVEN with the Extreme Ultraviolet Monitor and the neutral densities provided by the Mars Climate Database version 5.3, adapted to the conditions of the observations. We show that the altitude and the shape of the sample limb profiles are well reproduced using the Mars Climate Database neutral atmosphere. The simulated peak intensities of the CO_2^+ UVD and Cameron bands are in good agreement considering the uncertainties on the excitation cross sections and the calibration of the Imaging Ultraviolet Spectrograph (IUVS) and Extreme Ultraviolet Monitor instruments. No significant adjustment of the electron impact cross section on CO_2 to produce the $a^3\Pi$ state is needed. Seasonal-latitudinal maps of the Cameron and UVD peak altitude observed during two Martian years show variations as large as 23 km. Model simulations of the amplitude of these changes are in fair agreement with the observations except during the southern summer dust period (L_s = 270–320°) when the calculated rise of the dayglow layer is underestimated.

1. Introduction

The CO Cameron band system and CO_2^+ ultraviolet doublet (UVD) were first observed by Barth et al. (1971) during the Mariner 6 flyby of Mars. The CO Cameron bands range from 170 to 270 nm and correspond to the ($a^3\Pi \rightarrow X\ ^1\Sigma$) forbidden transition. The CO_2^+ UVD emission is observed at 298 and 299 nm and corresponds to the B ($^2\Sigma \rightarrow X\ ^2\Sigma$) transition. The altitude distribution and brightness of both emissions are mainly controlled by the CO_2 density and by the photoelectrons and solar photon fluxes impacting the Martian upper atmosphere. Therefore, the study of their distribution can provide information about the CO_2 distribution in the thermosphere and its variations. Earlier observations have been performed from the Mariner 6 and 7 flybys, the Mariner 9 orbiter, the Earth-orbiting Hopkins Ultraviolet Telescope, and Mars Express. Observed emission features included the HI 121.6 nm Lyman-α , NI 120.0 nm, OI 130.4 nm triplet and 135.6 nm doublet, the CO ($A^1\Pi - X^1\Sigma^+$) Fourth Positive bands, the CI 156.1 and 165.7 nm multiplets, Cameron bands, CO_2^+ ($B^2\Sigma - X^2\Pi$) UV doublet, OI 297.2 nm, the CO_2^+ ($A^2\Sigma^+ - X^2\Sigma^+$) Fox-Duffendack-Barker bands, and the N_2 ($A\ ^3\Sigma - X^1\Sigma$) Vegard-Kaplan emissions (Anderson & Hord, 1971; Barth et al., 1971, 1972; Conway, 1981; Cox et al., 2010; Feldman et al., 2000; Fox, 1992; Jain et al., 2015; Krasnopolsky & Feldman, 2002; Leblanc et al., 2006; Shematovich et al., 2008; Stevens et al., 2015; Simon et al., 2009; Stewart, 1972; Stewart et al., 1972; Strickland et al., 1973).

Earlier observations of the CO_2^+ UV doublet emission were reported by Stewart (1972) with the UV spectrometer on board Mariner. The altitude of the maximum brightness of the CO Cameron bands along the line of sight was 131 km. The limb intensity of the bands dropped by a factor of 2.5 between Mariner 6 and 7 and Mariner 9. This reduction was attributed to a decrease of the solar activity between the two sets of missions by Stewart et al. (1972). The latter also showed that the brightness of both band systems is well correlated with the $F_{10.7}$ cm solar flux, used as a proxy of the incident extreme ultraviolet (EUV) photon flux. Leblanc et al. (2006), Shematovich et al. (2008), and Simon et al. (2009) showed a few selected limb

profiles of both emissions observed with the SPectroscopy for the Investigation of the Characteristics of the Atmosphere of Mars

(SPICAM) instrument on board Mars Express. Leblanc et al. (2006) pointed out that the peak altitude of the Cameron bands measured by SPICAM at 117.5 km for $L_s < 130°$ was significantly lower than the 130 km measured with Mariner 9 UVS. They also found that the altitude of both emissions increased at $L_s > 130°$. A possible explanation was the presence of a global dust storm heating the lower atmosphere and moving up the altitude of the isobars in the thermosphere. Cox et al. (2010) analyzed the characteristics of the two emissions, their correlation, and dependence on the EUV solar flux during covering the 90° to 180° solar longitude season during Martian year 27. They found that the peak altitude of the CO_2^+ UVD is statistically located at 119.1 $\pm$ 7.0 km, on the average lower than the Cameron bands at 121.1 $\pm$ 6.5 km. They pointed out that both peak altitudes increased between $L_s = 140°$ and 180°, during a period characterized by an extensive dust storm. The linear correlation coefficient between their intensity was $r = 0.98$ and the mean Cameron/UVD ratio of 4.7, in close agreement with the 4.2 ratio found by Stewart et al. (1972). They also deduced that the brightness is essentially controlled by the solar zenith angle and the level of solar activity. González-Galindo et al. (2018) modeled the seasonal-latitudinal distribution of the two emissions using the ground-to-exosphere version of the general circulation model developed by the Laboratoire de Météorologie Dynamique (LMD). They compared their model predictions for Martian years 27 to 30 to limb observations from SPICAM and found a general good match with the observed peak altitudes, except during the period of global dust storm.

Observations used in this study have been performed with the Imaging Ultraviolet Spectrograph (IUVS) instrument on board the MAVEN spacecraft. In this study, the CO Cameron and the CO_2^+ doublet emissions are investigated in detail. We first describe the observation mode and the spatial coverage of the dayglow limb observations. We then make comparisons between airglow model simulations and a sample of observed limb scans. These comparisons confirm that the peak altitude is a good monitor of the changes in the CO_2 column density overlying the emission peak. We finally compare the observed seasonal-latitudinal altitude changes with those predicted by the Mars Climate Database (Forget et al., 1999; Millour et al., 2017).

2. IUVS Airglow Observations

The Imaging UltraViolet Spectrograph on board the MAVEN Mars orbiter has been operating since Fall 2014. During the period of observations used in this study, the spacecraft was on an elliptical orbit with a 6,000 km apoapsis and a periapsis near 160 km (Jakosky et al., 2015). IUVS supports two spectroscopic modes, with one of them operating near normal incidence and covering the 110–340 nm range with a resolving power ~250. It carries two detectors: a far ultraviolet (FUV) detector (115–190 nm) and a middle ultraviolet (MUV) detector (180–340 nm) with a spectral resolution of ~0.6 and 1.2 nm, respectively (McClintock et al., 2015). An Articulated Payload holding the instrument may be oriented in a direction depending on the location of MAVEN on its orbit and the mode of observation. It is equipped with a narrow slit ($11.3 \times 0.06°$) that intersects an instantaneous field of view whose projected size at the limb directly depends on the distance of MAVEN to the planet. In this study, we use limb scan observations that are collected when the spacecraft is below 500 km in order to guarantee adequate vertical resolution at the limb. The combination of the motion of the articulated platform and a scan mirror makes it possible to map out the vertical distribution of ultraviolet airglow emissions between 80 and 250 km. A maximum of 12 successive limb scans are collected during the 22 min of the periapsis phase. The IUVS slit is divided into seven spatial bins along the slit, so that seven limb profiles are obtained during each scan. These observations are binned into 5-km altitude bins and combined into a single limb profile.

IUVS can be operated in five different observation modes: stellar occultation, atmospheric limb scans, echelle, disk mapping, and Martian corona observations. In this work, we are interested in limb scan observations, and we use only the normal incidence spectroscopy that is divided in two channels: FUV and MUV. The dayglow emissions of interest here have been observed with the MUV channel at a spectral resolution of 1.2 nm. The absolute calibration of the spectra is based on laboratory tests as well as in-flight measurements using UV bright stars with well-known spectral fluxes as sources. For the MUV channel, the systematic uncertainties are estimated to be on the order of 25%. Additional details about the instrument properties and the observation modes are given in McClintock et al. (2015).

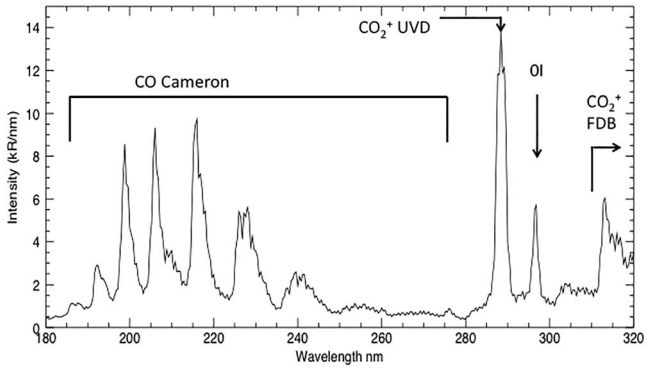

Figure 1. Average of 330 ultraviolet spectra based on limb scans collected with IUVS between 115 and 125 km during October 2015. The positions of the Cameron, CO_2^+ UVD and FDB bands, and the OI 297.2 nm emissions are indicated. The Cameron and UVD bands clearly stand out as bright dayglow features. FDB = Fox-Duffendack-Barker; UVD = ultraviolet doublet; IUVS = Imaging Ultraviolet Spectrograph.

The observations reported here were performed with the detector looking in a direction almost parallel to the surface. IUVS is equipped with a rotating mirror that allows 21 different positions so that it can perform limb observations at different altitudes as it passes close to or inside the atmosphere. Therefore, each mirror scan provides a limb profile of the different spectral features.

3. IUVS Observations

The observations used in this study were collected on the Martian dayside from 18 October 2014 and June 2018. They extend over a total period of two Martian years, from the southern summer in year 32 till southern summer of year 34. The latitudinal coverage at any specific solar longitude (L_s) is limited by the orbital and operational constraints, and no complete coverage is available at this time of the mission. The Level 1c/Version 13 IUVS data used in this study have been downloaded from National Aeronautics and Space Administration's Planetary Data System (PDS) archives. The PDS data provide calibrated brightness of individual emissions obtained by isolating emission features and spatial binning to facilitate processing. Each emission may be identified by its wavelength and expected relative intensity. The intensity of all identified features is determined by using a multiple linear regression method to fit the various components of each observed spectrum following convolution with the instrumental line spread function (Jain et al., 2015; Stevens et al., 2015). The very far wings of the point spread function contribute negligibly to signal (< 1%), and at that point other noise issues become more important, such as read noise and background subtraction. The contribution of scattered solar light is negligible for limb observations collected at tangent altitudes above ~100 km. The tangent altitude is calculated as the shortest distance between the line of sight and the areoid. A high signal-to-noise ratio average solar spectrum measured by IUVS instrument is used in the multiple linear regression analysis to calculate the brightness of various emissions provided in the level 1c data. The high intensity of the CO_2^+ UV doublet and Cameron bands and the high altitude of both emission layers make the scattered light contribution negligible.

Jain et al. (2015) and Gkouvelis et al. (2018) showed average MUV-MAVEN spectra collected at the limb. Figure 1 shows an example of the spectral region 180–330 nm obtained by averaging ~150 spectra. They were collected at tangent altitudes equal to 120 ± 5 km. Both the CO_2^+ ultraviolet doublet (CO_2^+ UVD) near 289 nm and the CO Cameron band between 175 and 270 nm dominate the Martian dayglow MUV spectrum. The OI emission at 297.2 nm, located between the CO_2^+ UV doublet and the Fox-Duffendack-Barker bands (Figure 1), was analyzed by Gkouvelis et al. (2018) who proposed to use it as a proxy of the latitude-seasonal change of the 43-nbar level.

Figure 2 shows examples of UV doublet and Cameron band altitude distribution, obtained by averaging individual limb profiles. The dates and locations are the same as the four cases presented by Gkouvelis et al. (2018) in their study of the O(^{1}S) airglow emission and listed in Table 1. These limb profiles correspond to the average of 112, 57, 50, and 72 limb scans for cases (a)–(d), respectively. They were collected at four different seasons at northern latitudes less than 35° and solar zenith angles less than 39°. They provide the mean limb intensity value in each 5-km bin and the 1-σ variability bar in blue. The statistical error is much less than the variability between limb scans and is not shown here. Following Gkouvelis et al.'s study, the maximum intensity and the peak altitude are determined with a 1-km accuracy by best fitting a second-order function to the data in the vicinity of the emission peak. The peak intensities range between 54 and 106 kR and the peak altitudes from 114 to 127 km. Table 1 lists the values of the peak altitude, intensity, and Cameron to UVS intensity ratio for each of the four panels shown in Figure 2. We note that airglow intensity values provided in the PDS archive version V13 have been recently revised, following additional in-orbit calibration measurements. The updated intensities have been corrected by a factor of 0.75 for the CO_2^+ UV bands and 0.85 for the Cameron bands. The systematic error is estimated to be on the order of 20%. These revised values have been adopted in this study. Similarly, the bottom four panels of Figure 2 show the corresponding average limb profiles of the CO Cameron bands. For this emission, the peak altitudes are a few

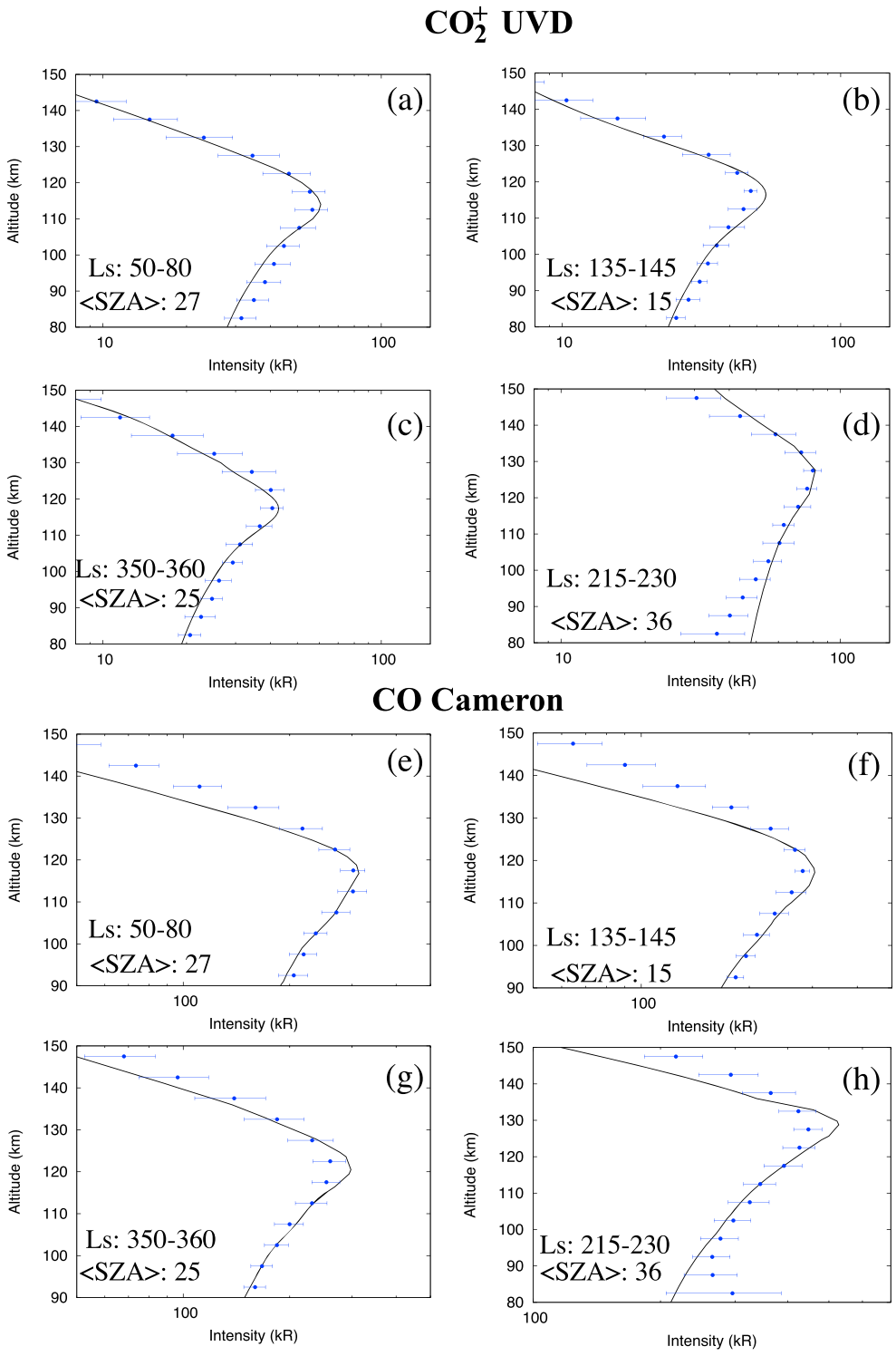

Figure 2. (a–d) Examples of average limb profiles of the CO_2^+ UVD dayglow corresponding to the conditions of the four cases described by Gkouvelis et al. (2018) and listed in Table 1. The blue horizontal bars indicate the 1-σ variability of the airglow intensity in each 5-km altitude bin. (e–h) Limb profiles of the CO Cameron band dayglow based on the same limb scans as the UVD examples. The black solid line shows the modeled limb profiles discussed in section 5.1. UVD = ultraviolet doublet.

Table 1
Observed Peak Altitudes and Limb Intensities of the Cameron and UVD Emissions in Figure 2

Case #	Date (mm/year)	Ls (deg)	Lat (deg)	UVD peak (km)	UVD peak (kR)	Cameron peak (km)	Cameron peak (kR)	Cam/UVD intensity	UVD intensity scaling factor[a]	Cameron bands scaling factor[a]
(a)	10/2015–11/2015	50–80	0–25	114	75	117	355	4.4	1.25	0.8
(b)	4/2016–5/2016	135–145	25–35	117	63	117	331	5.2	1.10	0.8
(c)	4/2017–5/2017	350–360	0–10	117	54	120	306	5.6	1.30	0.9
(d)	10/2014–11/2014	215–230	0–20	127	106	129	526	4.9	1.25	0.9

[a]Factors to be applied to the modeled intensity to match the observed peak brightness.

kilometers higher or lower than the simultaneous CO_2^+ UVD emission. The measured intensity ratio of the Cameron to the CO_2^+ UVD emission in these four cases ranges from 4.7 to 5.7 (Table 1), in close agreement with the mean value of 4.7 by Cox et al. (2010) based on measurements from SPICAM on board Mars Express. The variations in the brightness are essentially a response to the changing incident solar UV radiation due to solar activity and distance from the Sun. The altitude variations are mostly caused by changes in the overlying CO_2 column density that modifies the absorption of the solar FUV, EUV, and X-Ray radiations. Dust storms have also been shown to modify the thermal structure and the density of the Martian atmosphere up to the upper thermosphere (Bougher et al., 2017; Liu et al., 2018) and ionosphere (Withers & Pratt, 2013). General circulation models have also predicted large effects of increased atmospheric dust load on the thermospheric structure (Bougher et al., 2015; González-Galindo et al., 2015), including the vertical distribution of the CO_2 density. This point will be further discussed in section 5.

Cox et al.'s (2010) observations of the limb profiles of the Cameron bands and UV doublet have shown that the intensity and the altitude of the two features are closely correlated. Cox et al. obtained a correlation coefficient of 0.98 between the two sets of peak intensities for observations made with SPICAM-Mars Express during the L_s = 90–180° season. Similarly, the peak altitude covaried between 110 and 133 km, with a correlation coefficient of 0.98.

4. The Dayglow Model

The method used to calculate the CO_2^+ UVD and CO Cameron emission rates is adapted from the procedure described by Gkouvelis et al. (2018) to analyze the O(^{1}S-^{3}P) oxygen dayglow. The neutral atmosphere is provided by the MCD version 5.3 (Millour et al., 2017), which is based on the LMD model (Forget et al., 1999; González-Galindo et al., 2009). It uses the atmospheric dust load appropriate to Martian years 32, 33, and 34. The temperature and density profiles of CO_2, CO, and O are extracted for the conditions of cases (a) to (d) and used to calculate the limb intensity of the two airglow features. The CO_2 density is then scaled by an altitude-independent factor to minimize the difference between the observed and modeled airglow distribution.

The adopted wavelength dependence of the CO_2 absorption cross section is based on recent laboratory measurements and was described by Gkouvelis et al. (2018). The used values were recommended by Huestis and Berkovitz (2011), combined with the more recent high-resolution measurements between 87 and 110 nm by Archer et al. (2013). The variations of the absorption cross section with temperature at wavelengths shorter than 108 nm (the threshold wavelength for production of the Cameron bands by CO_2 photodissociation) have not been determined, and only measurements made close to room temperature are available. However, the temperature prevailing between 115 and 130 km in the Martian thermosphere range from ~100 to 160 K (Forget et al., 2009; Gröller et al., 2018), which may introduce some error in model calculations.

The transition from the $B^2\Sigma$ to the $X^2\Pi$ CO_2^+ ground state is permitted and produces a doublet at 288.3 and 289.6 nm. The double peak structure of the doublet is somewhat apparent in the IUVS average spectrum shown in Figure 1. The sources of the CO_2^+ UVD emission are (Fox, 1992)

$$CO_2 + h\nu\ (\lambda<69\ \text{nm}) \rightarrow CO_2^+\left(B^2\Sigma\right) + e_{ph} \quad (1)$$

$$CO_2 + e_{ph}\ (E>18.1\ \text{eV}) \rightarrow CO_2^+\left(B^2\Sigma\right) + e_{ph} + e'_{ph} \quad (2)$$

where hν designates solar EUV photons and e_{ph} and e'_{ph} are photoelectrons. Resonance scattering of CO_2^+ was estimated to contribute less than 4% by Fox and Dalgarno (1979) and will be neglected here.

The emission rate resulting from CO_2 photoionization into the CO_2^+ B ($^2\Sigma$) state is calculated from the total ionization cross section from Gallagher et al. (1988) multiplied by the wavelength-dependent quantum yield leading to the formation of the B state. This yield was calculated by Padial et al. (1981) and Avakyan et al. (1999). In this study, we use the quantum yield to the B state tabulated by Avakyan et al. (1999) that ranges from 14% to 23% of the absorption cross section between 0 and 70 nm. Carlson et al. (1973) measured the emission cross section into the CO_2^+ B state and the corresponding quantum yield relative to the CO_2 absorption cross section. These values are in rough agreement with those from by Padial et al. (1981) and Avakyan et al. (1999). The EUV solar flux reaching the top of the Martian atmosphere is provided by the reconstructed spectra (Thiemann et al., 2017) derived from the direct measurements by the EUV Monitor (EUVM, Eparvier et al., 2015) on board MAVEN during the same period.

The electron impact source (2) is calculated by folding the calculated photoelectron energy distribution function calculated by the Monte Carlo simulations with the cross section recommended by Itikawa (2002). Resonance scattering of solar UV radiation by CO_2^+ ions was shown to be negligible relative to (1) and (2) by Fox and Dalgarno (1979) on the basis of the low measured CO_2^+ ion density measured during the Viking descent (Hanson et al., 1977). The low CO_2^+ density is caused by rapid charge transfer with atomic oxygen converting CO_2^+ into O_2^+ ions. An important point for this study is that the production rates by processes (1) and (2) are directly proportional to the CO_2 local density in the thermosphere, which makes this emission a good proxy of CO_2 changes with location, season, and dust load conditions.

The radiative transition from the $a^3\Pi$ state to the CO ($X\,^1\Sigma$) ground state that produces the Cameron bands is spin forbidden. Its radiative lifetime is ~3 ms in the $v = 0$ level (Gilijamse et al., 2007). Excitation to the $a^3\Pi$ upper state takes place following several excitation processes (Fox, 1992):

$$CO_2 + h\nu\ (\lambda<108\ nm) \rightarrow CO\left(a^3\Pi\right) + O \quad (3)$$

$$CO_2 + e_{ph}\ (E>11.5\ eV) \rightarrow CO\left(a^3\Pi\right) + O + e_{ph} \quad (4)$$

$$CO + e_{ph}\ (E>6\ eV) \rightarrow CO\left(a^3\Pi\right) + O + e_{ph} \quad (5)$$

$$CO_2^+ + e_{th} \rightarrow CO\left(a^3\Pi\right) + O \quad (6)$$

where hν are solar EUV photons and e_{th} is a thermal electron.

The relative importance of these processes as sources of Cameron bands was discussed by Fox and Dalgarno (1979), Fox (1992), Leblanc et al. (2006), Shematovich et al. (2008), Cox et al. (2010), Gronoff et al. (2012), and Jain and Bhardwaj (2012) in relation to the dayglow measurements with SPICAM, and Gérard et al. (2015) for the Martian nightside aurora. The consensus view arising from those studies is that (3) and (4) are major sources of CO($a^3\Pi$) molecules. The photodissociation source (process 3) is calculated using the EUVM solar flux incident on the Martian atmosphere averaged over the period covering the acquisition of each average limb profile, the CO_2 absorption cross section, and the quantum yield into the CO $a^3\Pi$ state. We adopt the wavelength-dependent fractional yield relative to the total CO_2 absorption cross section between 85 and 109 nm measured by Lawrence (1972). The production by photoelectron impact on CO_2 is obtained by combining the photoelectron energy distribution function from the Monte Carlo model with the excitation cross section into the $a^3\Pi$ state. The electron impact cross section for the excitation of the Cameron system including cascade effects and its successive rescaling was discussed by Itikawa (2002). The uncertainties about the magnitude of the cross section of process (4) were discussed by Shematovich et al. (2008), Cox et al. (2010), Gronoff et al. (2012), and Jain and Bhardwaj (2012) in their comparisons with Mars Express SPICAM dayglow observations and more recently by Gérard et al. (2017) in the discussion of the Martian diffuse aurora. Along the lines of the conclusions from these studies, we use a peak value of 2.4×10^{-16} cm^2 suggested by Erdman and Zipf (1983), to account for the downward revision of the radiative lifetime of the CO $a^3\Pi$ state by Gilijamse et al. (2007). Unlike some of the earlier studies based on the SPICAM observations, we do not need to scale down the magnitude of this cross section by a factor of 2 to 3 to obtain good agreement with the IUVS observations, as will be shown in section 5. Dissociative recombination of CO_2^+ (6)

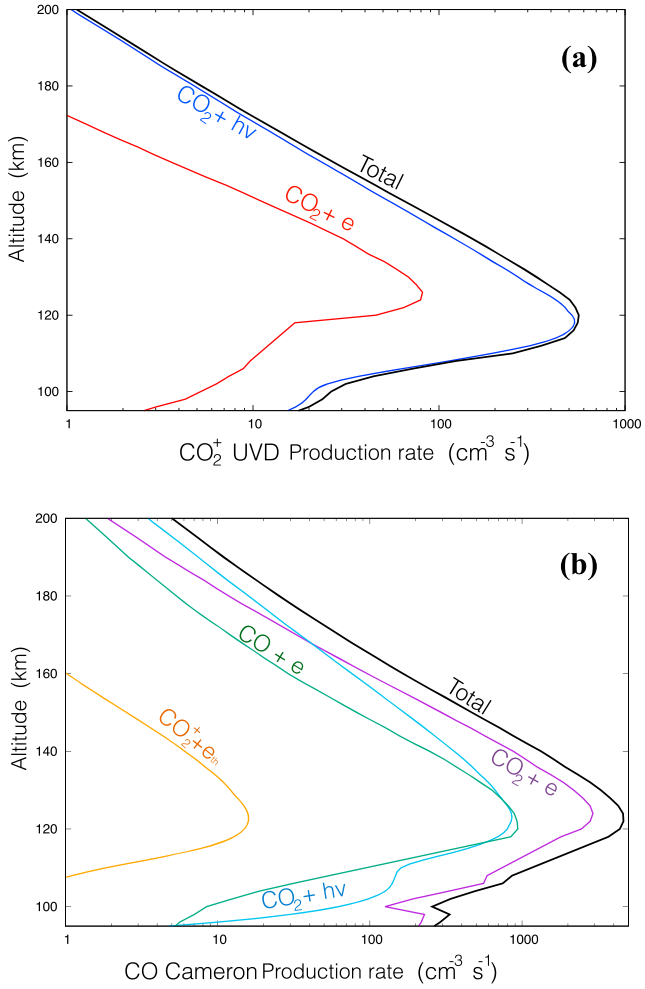

Figure 3. Calculated sources of CO_2^+ UV doublet (a) and CO Cameron (b) emissions for the conditions of case (a) in Figure 2. UVD = ultraviolet doublet.

is a minor source given the low CO_2^+ ion density and quantum efficiency of the channel producing CO in the $^3\Pi$ state. Figure 3 suggests that process (5) significantly contributes to the production of the CO $a^3\Pi$ state.

The calculated altitude dependence of the CO_2^+ UVD and CO Cameron production rates is shown in Figure 3. Figure 3a shows the strongly dominant role of (1) as a source of CO_2^+ B $^2\Sigma$ state. It shows that the photoionization contribution is about an order of magnitude larger than photoelectron impact at the peak altitude. Processes (1) and (2) directly involve photon or photoelectron interaction with CO_2 and represent nearly 100% of the UV doublet excitation rate. Process (4) (electron impact on CO_2) is the main source of CO $a^3\Pi$ state, followed by photodissociation of CO_2 (3) and electron impact on CO (5). The relative importance of photoelectron impact on CO molecules is directly dependent on the CO mixing ratio in the lower thermosphere. Process (5) contributes ~20% to the total $a^3\Pi$ state production rate near the emission peak in Figure 3b (case a), while its contribution was less in the simulations by Shematovich et al. (2008) with a similar model. The CO mixing ratio is variable (Clancy et al., 1983) and so is the contribution of process (5). The MCD, gives CO mixing ratios $f_{CO} = 7.8 \times 10^{-2}$, 4.4×10^{-2}, 3.3×10^{-2}, and 1.1×10^{-2} at 120 km for simulation cases (a) to (d), respectively. A value $f_{CO} = 2.5 \times 10^{-2}$ was measured by the Viking mass spectrometer (Nier & McElroy, 1977). We conducted a sensitivity test case where the CO mixing ratio for case (a) was divided by a factor of 10. In this case, the calculated Cameron peak intensity decreases by 19%. This would bring the modeled intensity in very close agreement with the observed peak values. Since the altitude of the peak of the CO_2^+ UVD emission solely depends on the CO_2 vertical density distribution, we use its variations as a proxy of the changes occurring in the CO_2 column density at and above the altitude of maximum emission.

5. Observations-Model Comparison

In this section, we compare the model simulations of the four averaged limb profiles shown in Figure 2. We examine the peak altitudes of the two emissions and their covariations. Finally, we build latitudinal-seasonal maps of the altitude of the Cameron and UVS emissions for comparison with the IUVS observations.

5.1. Comparison With IUVS Limb Observations

The calculated CO_2^+ UVD limb profiles corresponding to the four observed cases are shown in Figure 2 as solid black lines. All four simulated profiles are obtained by summing the contributions of processes (1) and (2) and integrating along the line of sight. The CO_2 density was varied to best match separately the individual Cameron and the UVS observed limb profiles shown in Figure 2. It was scaled up and down until the best agreement between the observed and the calculated peak altitudes was reached. As seen in Figure 2, the comparisons indicate that the model matches the observations of the emission peak altitude within 1 km or less. The CO_2 density scaling factors (relative to the MCD values) applied to best match the CO_2^+ UVD peak intensity are 1.0 for cases (a) and (b), 1.2 for case (c), and 1.4 for case (d). In a second step, the calculated emission profile was scaled as a whole by a constant factor to best fit the observed intensity (Table 1). The brightness scaling factors are 1.25, 1.10, 1.30, and 1.25, respectively for cases (a)–(d). The average scaling by a factor of 1.22 is well within the combined uncertainties of the CO_2 ionization cross section, the branching ratio for emission from the CO_2^+ B state and the IUVS absolute calibration.

Figure 2 also compares the simulated limb intensity of the CO Cameron bands for the same four cases as the CO_2^+ UVD emission. The limb profiles illustrated in Figures 2e to 2h are calculated with the same CO_2

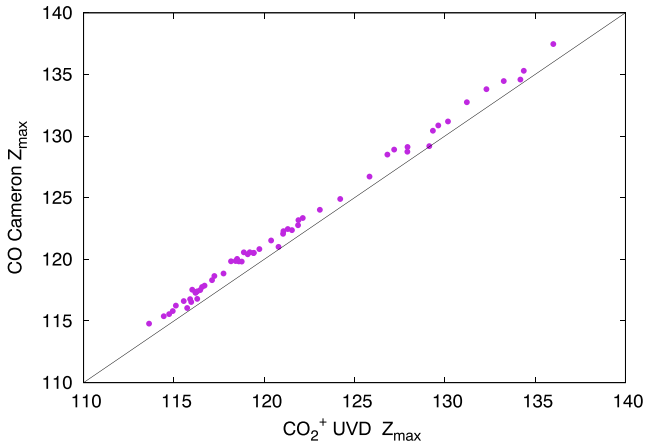

Figure 4. Observed peak altitude of the CO Cameron plotted versus the altitude of the CO_2^+ limb profiles for each of the latitude-solar longitude pixels. The solid line indicates equal values of the two altitudes. UVD = ultraviolet doublet.

density scaling coefficients as for the CO_2^+ UV doublet, since numerical tests have shown that CO_2 density adjustments for best fit peak altitudes are the same as for the UVD. The plots indicate that the calculated peak altitudes of the Cameron bands also agree with the IUVS observations within a 1-km accuracy. For the Cameron bands, the intensity scaling factors were 0.8 for cases (e) and (f) and 0.9 for cases (g) and (h), also within the uncertainties in the cross sections leading to the production of the CO $a^3\Pi$ state.

Unlike earlier studies, no adjustment of the electron impact dissociative excitation of CO_2 by photoelectrons (process 3) was applied to obtain satisfactory agreement with the observations. One possibility is that the measurements modeled in this situ were collected with the IUVS instrument, whereas previous airglow model comparisons were made with observations from the SPICAM instrument on board Mars Express. Comparisons between the limb intensities of the Cameron bands collected during the two missions indicate that they do not agree, even if they were made at similar solar activity level. For example, Jain et al. (2015) showed in their Table 1 that the Cameron band limb intensity measured with IUVS is a factor of 2.8 larger than the SPICAM/Mars Express (MEx) value for a similar solar activity level ($F_{10.7}$ index = 105–110). This, by itself, would explain why studies based on SPICAM observations needed to divide the e + CO_2 excitation cross section by a factor of 2 to 3, while this correction is not required to match the IUVS observations. In addition, the EUV solar flux interacting with the Martian atmosphere is now much better determined than in earlier studies, as it is measured from Mars orbit concurrently with the airglow observations. Uncertainties about the magnitude of this cross section are of no consequence on this study that concentrates on the seasonal-latitudinal changes of altitude of the CO_2^+ UVD and Cameron band emissions. These changes are independent of the magnitude of the e + CO_2 excitation cross section, but they only depend on the solar flux absorption by CO_2.

In these simulations, electron dissociative excitation of CO is a significant source of CO $a^3\Pi$ state, resulting from the relatively large CO mixing ratio provided by the MCD in the region of the Cameron region of emission. As a test, we arbitrarily decreased the CO density profile by an order of magnitude. In this case, the calculated total intensities are in very close agreement with the observed peak values. In any case, as noted before, given the accumulation of errors on the IUVS intensities and cross sections, solar EUV flux, and neutral model uncertainties, a perfect match with the observations is not expected.

We conclude that the airglow model adequately reproduces the CO_2^+ UV doublet observations, especially the altitude of the peak. The Cameron bands with their multiple sources and the uncertainties on the CO density are a somewhat less reliable indicator of the CO_2 density.

5.2. Observed and Calculated Emission Altitude Changes

We have constructed maps of the latitudinal-seasonal distribution of the peak of both emissions for all IUVS observations since the beginning of the operational period of the MAVEN mission. For this purpose, we first define solar longitude-latitude bins of 15° × 15° for a given range of solar zenith angles or local times. The limb profiles collected during the corresponding time period are summed and averaged in order to create smoothed limb distributions in each bin. The tangent altitude of the emission peak at the limb in each pixel is then determined following the method described in Gkouvelis et al. (2018) and assigned to the corresponding map pixel.

In agreement with the model simulations, the peak altitudes of the two emissions are strongly correlated. This is clearly demonstrated in Figure 4 showing the peak altitude of the limb profiles of the Cameron bands as a function of that of the corresponding CO_2^+ profiles for each latitude-solar longitude pixel. The plot clearly indicates that the two quantities covary. The correlation coefficient between the altitude of corresponding pixels in the UVD and Cameron maps is equal to 0.99 at a confidence of over 99% based on the Fisher law. This strong covariation strongly suggests that both emissions respond to a common change in

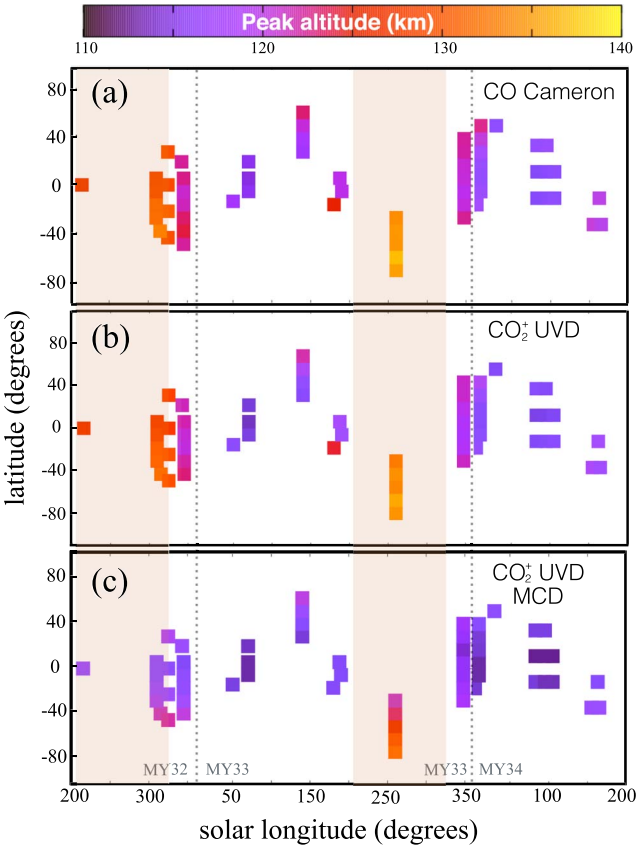

Figure 5. Latitude-solar longitude maps of the observed peak altitude of the Cameron bands (a), the CO_2^+ UVD (b), and the simulated CO_2^+ UVD (c) for solar zenith angles less than 40°. The dust season is indicated by the brown stripes between 220° and 310° solar longitudes. UVD = ultraviolet doublet.

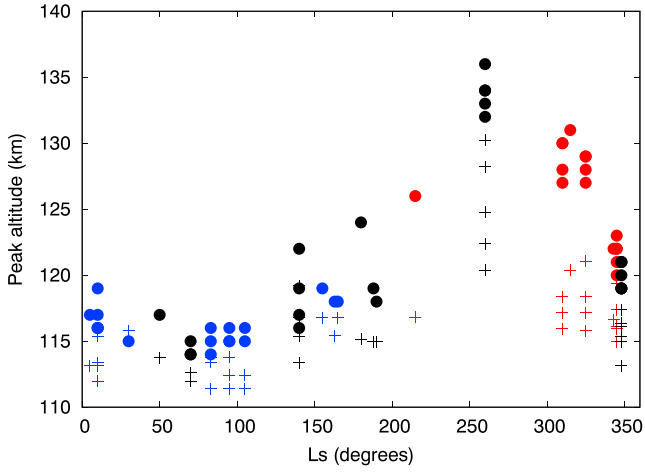

Figure 6. Comparative seasonal evolution of the peak altitude of the CO_2^+ UVD dayglow measured by IUVS (dots) with the calculated altitudes (cross) during several Martian years. The red, black, and blue colors are used to indicate Martian years 32, 33, and 34 accordingly. UVD = ultraviolet doublet; IUVS = Imaging Ultraviolet Spectrograph.

the atmospheric structure, essentially a vertical redistribution of the CO_2 density. The distance of the data points relative to the bisector (line of equal peak altitude) indicates that the maximum emission of the Cameron bands is slightly (~1 to 2 km) higher than the CO_2^+ UVD bands. An average altitude offset of 2.4 km was found by Cox et al. (2010) in their study of the SPICAM observations of the two emissions. Since the altitude of the two emissions covary and because the two CO_2^+ UVD sources are both directly related to the CO_2 density distribution, we mainly concentrate on the comparison between the observed and simulated CO_2^+ UV doublet emission.

Figure 5 shows the altitude map based on IUVS limb observations at a solar zenith angle limited to less than 40° to minimize the effect of changing solar zenith angle. The maps exhibit several interesting features. First, the peak altitudes of both emissions exhibit variations by as much as 30 km between the low values near L_s = 70° at low latitudes and the highest altitudes at 260° in the southern hemisphere. Second, the largest change is observed between the series of data points at 260° and the following group of observations at L_s = 350°. This period and location correspond to an increased airborne dust load at 610 Pa in the Martian atmosphere derived from the infrared optical depth measurements from various spacecraft (Montabone et al., 2015). Simulations for MY 34 are based on the MCD climatology scenario for solar minimum conditions appropriate to this period (Millour et al., 2017), as the atmospheric dust load is not available for LMD simulation at the time of writing. Figure 5 c shows the altitude map of the CO_2^+ UVD emission peak calculated for the same latitudinal-seasonal pixels as Figure 5b calculated using the source processes discussed in section 4 and the MCD model atmosphere.

The mean quantities characterizing each filled pixel in Figure 5 (latitude, solar longitude, EUV solar flux, and MCD neutral atmosphere) are used as inputs to the model, and the calculated volume emission rate is numerically integrated along the line of sight. Finally, the emission peak is located to determine the altitude value assigned to each pixel. We note that the calculated altitude of the emission peak is in close agreement with the observations in L_s sectors 0–190° and near 350°. In contrast, the altitude rise of the emission peak is less than the observed one by up to 15 km. The variability of the simulated altitude (~12 km) is less than in the observations (~23 km). Although they follow the same pattern, the altitude variations are more pronounced in the IUVS observations between the fall equinox and southern winter seasons than during the other half Martian year. This is confirmed by Figure 6 comparing the evolution of the Cameron bands (a) and UVD (b) peak altitudes observed during two Martian years by IUVS with the simulated values (c). It clearly shows how the measured dayglow altitudes diverge from the calculated values after L_s = 200°. The data gaps in the dayglow coverage of these two groups of observations correspond to the passage of Mars near perihelion (270°) near summer solstice in the southern hemisphere. Third, we note that the highest peak altitudes are observed at low latitudes near L_s = 300 and 350° during Martian year 32 and in the southern hemisphere between 250 and 265°. These periods correspond to the dust season, as indicated by the brown stripes in Figure 5. The atmospheric dust load perturbs the interaction of the solar radiation that modifies the atmospheric thermal structure and thus the vertical distribution of the CO_2 density.

6. Discussion and Conclusions

We first note that the main characteristics of the two emissions observed with MAVEN/IUVS fully agree with the conclusions of earlier work based on the Mariner and Mars Express ultraviolet dayglow observations. Figure 4 clearly indicates that the peak altitude and the peak brightness of the two emissions covary with a slight offset of about 2 km. Second, CO_2 is the main constituent controlling the production of excited CO_2^+ ions since it is directly involved in the two source processes.

Unlike earlier studies, the Cameron bands peak intensity is reproduced within 20% using the electron impact on CO_2 cross section recommended by Shirai et al. (2001), based on the renormalization by Erdman and Zipf (1983). At least part of the difference with previous studies stems from the higher Cameron band intensity observed by IUVS for a given range of solar zenith angle. In our four examples (a) to (d), the intensity ranges between 282 and 526 kR (Table 1). These values are substantially larger than the 50 to 175 kR derived from SPICAM by Jain et al. (2015) for similar solar zenith angles. However, both data sets covered approximately the declining phase of the solar cycle and the same range of F_{107} solar activity index (105 to 110). In addition, the EUV solar flux interacting with the Martian atmosphere is now much better determined than previously as it is measured from Mars orbit simultaneously with the airglow observations.

In this study, we show for the first time that the peak altitudes of both CO Cameron bands and CO_2^+ UV doublet respond to changing seasons and latitudes and atmospheric dust load. These variations cannot directly stem from changing solar irradiation whose absolute flux has no direct influence on the altitude of maximum emission. Instead, they are produced by changes in the Martian atmospheric content of CO_2. These changes result from perturbations of the thermal structure that modify the vertical distribution of the CO_2 density.

Large seasonal changes have been observed in the surface total pressure (Hess et al., 1980) with the maximum value observed between near perihelion (L_s = 220–320°). These seasonal variations are caused by the asymmetric exchange of CO_2 between the atmosphere and the winter polar caps, resulting in addition or subtraction of carbon dioxide from the atmosphere. In this work, we observe the highest peak altitude of both CO_2^+ and Cameron band emissions near perihelion, corresponding to an upward displacement of the isobars during this season. Changes in the altitude of isobars have also been observed in the upper atmosphere using other techniques. For example, our observations are consistent with the increase of the CO_2 density observed at fixed altitudes using the stellar occultation method with the SPICAM (Forget et al., 2009) and IUVS (Gröller et al., 2018) spectrographs. The CO_2 density increased by a factor as large as 20 at 120–130 km. This amplitude exceeded by a factor ~5 of the CO_2 density variations predicted by the LMD model. The change of CO_2 density at 120 km by a factor of ~20 observed in the solar occultation measurements corresponds to an altitude increase of ~20 km of the isobar level. This is in close agreement with the observed rise of both CO_2^+ UVD and CO Cameron peak altitudes from 115 to 135 km described in Figure 6.

MAVEN-IUVS observations indicate that the altitude of the emission peaks of both emissions changes with latitude and season. The peak altitude rises during summer in the southern hemisphere (L_s = ~200 to 320°). Our model simulations based on the MCD neutral atmosphere for Martian years 32 and 33 also predict seasonal variations in the thermosphere up to the exobase Figure 6c. The general good agreement between the observed and simulated limb profiles of both emissions indicates that the MCD CO_2 density distribution in the 120- to 130-km region from the MCD is adequate to model the dayglow peak altitude at least in the absence of global dust storm. During dust storm periods, the altitude of the peak dayglow emissions moves up with larger amplitude than predicted by the MCD. The peak altitude of the two emissions was also modeled as a function of the solar longitude by González-Galindo et al. (2018) for different Martian years than analyzed in this work. González-Galindo et al. (2018) found that the upward displacement of the altitude of the airglow layers predicted by the MCD during dust seasons was less than the SPICAM observations by as much as 16 km. In this study, we confirm the inability of the MCD to predict the amplitude of the change of the emission peak altitude during dust seasons observed with MAVEN/IUVS.

List of Acronyms

EUVM	Extreme UltraViolet Monitor on board the MAVEN orbiter
IUVS	Imaging UltraViolet Spectrograph on board the MAVEN orbiter
Ls	Planetary solar longitude
MAVEN	Mars Atmosphere and Volatile EvolutioN spacecraft orbiting Mars
MCD	Mars Climate Database
M-GITM	Mars Global Ionosphere-Thermosphere Model
SPICAM	SPectroscopy for the Investigation of the Characteristics of the Atmosphere of Mars on board the Mars Express orbiter
UVD	Ultraviolet doublet emission associated with the B $^2\Sigma \rightarrow$ X $^2\Sigma$ transition of CO_2^+

Acknowledgments
This research was partly funded by the NOMAD PRODEX program managed by the European Space Agency with the help of the Belgian Science Policy Office (BELSPO) and the BELSPO's SCOOP/BRAIN research contract. B. H. is supported by the Belgian Fund for Scientific Research (FNRS). We thank E. Millour for his help in using the MCD. The IUVS and EUVM MAVEN data sets were obtained from NASA's Planetary Data System (PDS) available at http://atmos.nmsu.edu/data_and_services/atmospheres_data/MAVEN/maven_main.html. The IUVS archives level V13 were used for this study. The Mars Climate Database (version 5.3) is available online at http://www-mars.lmd.jussieu.fr/mcd_python/. This work utilized the RMACC Summit supercomputer, which is supported by the National Science Foundation (awards ACI-1532235 and ACI-1532236), the University of Colorado Boulder, and Colorado State University. The Summit supercomputer is a joint effort of the University of Colorado Boulder and Colorado State University.

References

Anderson Jr., D. E., & Hord, C. W. (1971). MMariner 6 and 7 ultraviolet spectrometer experiment: Analysis of hydrogen Lyman-alpha data. *Journal of Geophysical Research*, *76*(28) 6666–6673.

Archer, L. E., Stark, G., Smith, P. L., Lyons, J. R., De Oliveira, N., Nahon, L., et al. (2013). Room temperature photoabsorption cross section measurements of CO_2 between 91,000 and 115,000 cm^{-1}. *Journal of Quantitative Spectroscopy and Radiative Transfer*, *117*, 88–92. https://doi.org/10.1016/j.jqsrt.2012.11.009

Avakyan, S. V., Ii'In, R. N., Lavrov, V. M., & Ogurtsov, G. N. (1999). *Collision processes and excitation of UV emission from planetary atmospheric gases: A handbook of cross sections*. Amsterdam: CRC Press.

Barth, C. A., Hord, C. W., Pearce, J. B., Kelly, K. K., Anderson, G. P., & Stewart, A. I. (1971). Mariner 6 and 7 ultraviolet spectrometer experiment: Upper atmosphere data. *Journal of Geophysical Research*, *76*(10), 2213–2227. https://doi.org/10.1029/JA076i010p02213

Barth, C. A., Stewart, A. I., Hord, C. W., & Lane, A. L. (1972). Mariner 9 ultraviolet spectrometer experiment: Mars airglow spectroscopy and variations in Lyman alpha. *Icarus*, *17*(2), 457–468. https://doi.org/10.1016/0019-1035(72)90011-5

Bougher, S. W., Pawlowski, D., Bell, J. M., Nelli, S., McDunn, T., Murphy, J. R., et al. (2015). Mars Global Ionosphere-Thermosphere Model: Solar cycle, seasonal, and diurnal variations of the Mars upper atmosphere. *Journal of Geophysical Research: Planets*, *120*, 311–342. https://doi.org/10.1002/2014JE004715

Bougher, S. W., Roeten, K. J., Olsen, K., Mahaffy, P. R., Benna, M., Elrod, M., et al. (2017). The structure and variability of Mars dayside thermosphere from MAVEN NGIMS and IUVS measurements: Seasonal and solar activity trends in scale heights and temperatures. *Journal of Geophysical Research: Space Physics*, *122*, 1296–1313. https://doi.org/10.1002/2016JA023454

Carlson, R. W., Judge, D. L., & Ogawa, M. (1973). Photoionization of the CO_2^+ ($B^2\Sigma_u^+$ $X^2\Pi_g$) 2980-A band. *Journal of Geophysical Research*, *78*(16), 3194–3196. https://doi.org/10.1029/JA078i016p03194

Clancy, R. T., Muhleman, D. O., & Jakosky, B. M. (1983). Variability of carbon monoxide in the Mars atmosphere. *Icarus*, *55*(2), 282–301. https://doi.org/10.1016/0019-1035(83)90083-0

Conway, R. R. (1981). Spectroscopy of the Cameron bands in the Mars airglow. *Journal of Geophysical Research*, *86*(A6), 4767–4775. https://doi.org/10.1029/JA086iA06p04767

Cox, C., Gérard, J. C., Hubert, B., Bertaux, J. L., & Bougher, S. W. (2010). Mars ultraviolet dayglow variability: SPICAM observations and comparison with airglow model. *Journal of Geophysical Research*, *115*, E04010. https://doi.org/10.1029/2009JE003504

Eparvier, F. G., Chamberlin, P. C., Woods, T. N., & Thiemann, E. M. B. (2015). The solar extreme ultraviolet monitor for MAVEN. *Space Science Reviews*, *195*(1-4), 293–301. https://doi.org/10.1007/s11214-015-0195-2

Erdman, P. W., & Zipf, E. C. (1983). Electron-impact excitation of the Cameron system (a3Π → X1Σ) of CO. *Planetary and Space Science*, *31*(3), 317–321. https://doi.org/10.1016/0032-0633(83)90082-X

Feldman, P. D., Burgh, E. B., Durrance, S. T., & Davidsen, A. F. (2000). Far-ultraviolet spectroscopy of Venus and Mars at 4 Å resolution with the Hopkins Ultraviolet Telescope on Astro-2. *The Astrophysical Journal*, *538*(1), 395–400. https://doi.org/10.1086/309125

Forget, F., Hourdin, F., Fournier, R., Hourdin, C., Talagrand, O., Collins, M., et al. (1999). Improved general circulation models of the Martian atmosphere from the surface to above 80 km. *Journal of Geophysical Research*, *104*(E10), 24,155–24,175. https://doi.org/10.1029/1999JE001025

Forget, F., Montmessin, F., Bertaux, J. L., González-Galindo, F., Lebonnois, S., Quemerais, E., et al. (2009). Density and temperatures of the upper Martian atmosphere measured by stellar occultations with Mars Express SPICAM. *Journal of Geophysical Research*, *114*, E01004. https://doi.org/10.1029/2008JE003086

Fox, J. L. (1992). Airglow and aurora in the atmospheres of Venus and Mars. In *Venus and Mars: Atmospheres, ionospheres, and solar wind interactions*, *Geophysical monograph series*, (pp. 191–222). Washington, D. C: American Geophysical Union. https://doi.org/10.1029/GM066p0191

Fox, J. L., & Dalgarno, A. (1979). Ionization, luminosity, and heating of the upper atmosphere of Mars. *Journal of Geophysical Research*, *84*(A12), 7315–7333. https://doi.org/10.1029/JA084iA12p07315

Gallagher, J. W., Brion, C. E., Samson, J. A. R., & Langhoff, P. W. (1988). Absolute cross sections for molecular photoabsorption, partial photoionization, and ionic photofragmentation processes. *Journal of Physical and Chemical Reference Data*, *17*(1), 9–153. https://doi.org/10.1063/1.555821

Gérard, J. C., Soret, L., Libert, L., Lundin, R., Stiepen, A., Radioti, A., & Bertaux, J. L. (2015). Concurrent observations of ultraviolet aurora and energetic electron precipitation with Mars Express. *Journal of Geophysical Research: Space Physics*, *120*, 6749–6765. https://doi.org/10.1002/2015ja021150

Gérard, J.-C., Soret, L., Shematovich, V. I., Bisikalo, D. V., & Bougher, S. W. (2017). The Mars diffuse aurora: A model of ultraviolet and visible emissions. *Icarus*, *288*, 284–294. https://doi.org/10.1016/j.icarus.2017.01.037

Gilijamse, J. J., Hoekstra, S., Meek, S. A., Metsälä, M., van de Meerakker, S. Y. T., Meijer, G., & Groenenboom, G. C. (2007). The radiative lifetime of metastable CO ($a^3\Pi$, n = 0). *The Journal of Chemical Physics*, *127*(22), 221102-1–221102-4. https://doi.org/10.1063/1.2813888

Gkouvelis, L., Gérard, J.-C., Ritter, B., Hubert, B., Schneider, N. M., & Jain, S. (2018). The O(1S) 297.2 nm dayglow emission: A tracer of CO_2 density variations in the Martian lower thermosphere. *Journal of Geophysical Research: Planets*, *123*, 3119–3132. https://doi.org/10.1029/2018JE005709

González-Galindo, F., Chaufray, J.-Y., Forget, F., Garcia-Comas, M., Montmessin, F., Jain, S. K., & Stiepen, A. (2018). UV dayglow variability on Mars: Simulation with a global climate model and comparison with SPICAM/MEx data. *Journal of Geophysical Research: Planets*, *123*, 1934–1952. https://doi.org/10.1029/2018JE005556

González-Galindo, F., Forget, F., López-Valverde, M. A., Angelats, i., Coll, M., & Millour, E. (2009). A ground-to-exosphere Martian general circulation model: 1. Seasonal, diurnal, and solar cycle variation of thermospheric temperatures. *Journal of Geophysical Research*, *114*, E04001. https://doi.org/10.1029/2008JE003246

González-Galindo, F., López-Valverde, M. A., Forget, F., García-Comas, M., Millour, E., & Montabone, L. (2015). Variability of the Martian thermosphere during eight Martian years as simulated by a ground-to-exosphere global circulation model. *Journal of Geophysical Research: Planets*, *120*, 2020–2035. https://doi.org/10.1002/2015JE004925

Gröller, H., Montmessin, F., Yelle, R. V., Lefèvre, F., Forget, F., Schneider, N. M., et al. (2018). MAVEN/IUVS stellar occultation measurements of Mars atmospheric structure and composition. *Journal of Geophysical Research: Planets*, *123*, 1449–1483. https://doi.org/10.1029/2017JE005466

Gronoff, G., Simon Wedlund, C., Mertens, C. J., Barthélemy, M., Lillis, R. J., & Witasse, O. (2012). Computing uncertainties in ionosphere-airglow models: II. The Martian airglow. *Journal of Geophysical Research*, *117*, A05309. https://doi.org/10.1029/2011JA017308

Hanson, W. B., Sanatani, S., & Zuccaro, D. R. (1977). The Martian ionosphere as observed by the Viking retarding potential analyzers. *Journal of Geophysical Research*, *82*(28), 4351–4363. https://doi.org/10.1029/JS082i028p04351

Hess, S. L., Ryan, J. A., Tillman, J. E., Henry, R. M., & Leovy, C. B. (1980). The annual cycle of pressure on Mars measured by Viking landers 1 and 2. *Geophysical Research Letters*, *7*(3), 197–200. https://doi.org/10.1029/GL007i003p00197

Huestis, D. L., & Berkowitz, J. (2011). Critical Evaluation of the Photoabsorption Cross Section of CO_2 from 0.125 to 201.6 nm a Room Temperature. *Advances in GeosciencesAdvances in Geosciences* (pp. 229–242).

Itikawa, Y. (2002). Cross sections for electron collisions with carbon dioxide. *Journal of Physical and Chemical Reference Data*, *31*(3), 749–767. https://doi.org/10.1063/1.1481879

Jain, S. K., & Bhardwaj, A. (2012). Impact of solar EUV flux on CO Cameron band and CO_2^+ UV doublet emissions in the dayglow of Mars. *Planetary and Space Science*, *63*, 110–122.

Jain, S. K., Stewart, A. I. F., Schneider, N. M., Deighan, J., Stiepen, A., Evans, J. S., et al. (2015). The structure and variability of Mars upper atmosphere as seen in MAVEN/IUVS dayglow observations. *Geophysical Research Letters*, *42*, 9023–9030. https://doi.org/10.1002/2015GL065419

Jakosky, B. M., Lin, R. P., Grebowsky, J. M., Luhmann, J. G., Mitchell, D. F., Beutelschies, G., et al. (2015). The Mars atmosphere and volatile evolution (MAVEN) mission. *Space Science Reviews*, *195*(1-4), 3–48. https://doi.org/10.1007/s11214-015-0139-x

Krasnopolsky, V. A., & Feldman, P. D. (2002). Far ultraviolet spectrum of Mars. *Icarus*, *160*(1), 86–94. https://doi.org/10.1006/icar.2002.6949

Lawrence, G. M. (1972). Photodissociation of CO_2 to produce CO (a $^3\Pi$). *The Journal of Chemical Physics*, *56*(7), 3435–3442. https://doi.org/10.1063/1.1677717

Leblanc, F., Chaufray, J. Y., Lilensten, J., Witasse, O., & Bertaux, J. L. (2006). Martian dayglow as seen by the SPICAM UV spectrograph on Mars Express. *Journal of Geophysical Research*, *111*, E09S11. https://doi.org/10.1029/2005JE002664

Liu, G., England, S. L., Lillis, R. J., Withers, P., Mahaffy, P. R., Rowland, D. E., et al. (2018). Thermospheric expansion associated with dust increase in the lower atmosphere on Mars observed by MAVEN/NGIMS. *Geophysical Research Letters*, *45*, 2901–2910. https://doi.org/10.1002/2018GL077525

McClintock, W. E., Schneider, N. M., Holsclaw, G. M., Clarke, J. T., Hoskins, A. C., Stewart, I., et al. (2015). The imaging ultraviolet spectrograph (IUVS) for the MAVEN mission. *Space Science Reviews*, *195*(1-4), 75–124. https://doi.org/10.1007/s11214-014-0098-7

Millour, E., Forget, F., Spiga, A., Vals, M., Zakharov, V., Navarro, T., et al. (2017). The Mars Climate Database (MCD version 5.3). In EGU General Assembly Conference Abstracts (Vol. 19, p. 12247).

Montabone, L., Forget, F., Millour, E., Wilson, R. J., Lewis, S. R., Cantor, B., et al. (2015). Eight-year climatology of dust optical depth on Mars. *Icarus*, *251*, 65–95. https://doi.org/10.1016/j.icarus.2014.12.034

Nier, A. O., & McElroy, M. B. (1977). Composition and structure of Mars' upper atmosphere: Results from the neutral mass spectrometers on Viking 1 and 2. *Journal of Geophysical Research*, *82*(28), 4341–4349. https://doi.org/10.1029/JS082i028p04341

Padial, N., Csanak, G., McKoy, B. V., & Langhoff, P. W. (1981). Photoexcitation and ionization in carbon dioxide: Theoretical studies in the separated-channel static-exchange approximation. *Physical Review A*, *23*(1), 218–235. https://doi.org/10.1103/PhysRevA.23.218

Shematovich, V. I., Bisikalo, D. V., Gérard, J.-C., Cox, C., Bougher, S. W., & Leblanc, F. (2008). Monte Carlo model of electron transport for the calculation of Mars dayglow emissions. *Journal of Geophysical Research*, *113*, E02011. https://doi.org/10.1029/2007JE002938

Shirai, T., Tabata, T., & Tawara, H. (2001). Analytic cross sections for electron collisions with CO, CO_2, and H_2O relevant to edge plasma impurities. *Atomic Data and Nuclear Data Tables*, *79*(1), 143–184. https://doi.org/10.1006/adnd.2001.0866

Simon, C., Witasse, O., Leblanc, F., Gronoff, G., & Bertaux, J. L. (2009). Dayglow on Mars: Kinetic modelling with SPICAM UV limb data. *Planetary and Space Science*, *57*(8-9), 1008–1021. https://doi.org/10.1016/j.pss.2008.08.012

Strickland, D. J., Stewart, A. I., Barth, C. A., Hord, C. W., Lane, A. L. (1973). Mariner 9 ultraviolet spectrometer experiment: Mars atomic oxygen 1304-A emission. *Journal of Geophysical Research*, *78*(22) 4547–4559.

Stevens, M. H., Evans, J. S., Schneider, N. M., Stewart, A. I. F., Deighan, J., Jain, S. K., et al. (2015). New observations of molecular nitrogen in the Martian upper atmosphere by IUVS on MAVEN. *Geophysical Research Letters*, *42*, 9050–9056. https://doi.org/10.1002/2015GL065319

Stewart, A. I. (1972). Mariner 6 and 7 ultraviolet spectrometer experiment: Implications of CO_2^+, CO and O airglow. *Journal of Geophysical Research*, *77*(1), 54–68. https://doi.org/10.1029/JA077i001p00054

Stewart, A. I., Barth, C. A., Hord, C. W., & Lane, A. L. (1972). Mariner 9 ultraviolet spectrometer experiment: Structure of Mars' upper atmosphere. *Icarus*, *17*(2), 469–474. https://doi.org/10.1016/0019-1035(72)90012-7

Thiemann, E., Chamberlin, P. C., Eparvier, F. G., Templeman, B., Woods, T. N., Bougher, S. W., & Jakosky, B. M. (2017). The MAVEN EUVM model of solar spectral irradiance variability at Mars: Algorithms and results. *Journal of Geophysical Research: Space Physics*, *122*, 2748–2767. https://doi.org/10.1002/2016JA023512

Withers, P., & Pratt, R. (2013). An observational study of the response of the upper atmosphere of Mars to lower atmospheric dust storms. *Icarus*, *225*(1), 378–389. https://doi.org/10.1016/j.icarus.2013.02.032